Mon. Not. R. Astron. Soc. **358,** 860–868 (2005) doi:10.1111/j.1365-2966.2005.08791.x

Rapid variability of the arcsec-scale X-ray jets of SS 433

S. Migliari,[1⋆] R. P. Fender,[1,2] K. M. Blundell,[3] M. Méndez[4] and M. van der Klis[1]

[1]*Astronomical Institute 'Anton Pannekoek', University of Amsterdam, and Center for High Energy Astrophysics, Kruislaan 403, 1098 SJ, Amsterdam, the Netherlands*
[2]*Department of Physics and Astronomy, University of Southampton, Hampshire SO17 1BJ*
[3]*Astrophysics, University of Oxford, Denys Wilkinson Building, Keble Road, Oxford OX1 3RH*
[4]*SRON, National Institute for Space Research, 3584 CA, Utrecht, the Netherlands*

Accepted 2005 January 5. Received 2005 January 5; in original form 2004 June 4

ABSTRACT

We present X-ray images of all the available *Chandra* observations of the galactic jet source SS 433. We have studied the morphology of the X-ray images and inspected the evolution of the arcsec X-ray jets, recently found to be manifestations of *in situ* reheating of the relativistic gas downstream in the jets. The *Chandra* images reveal that the arcsec X-ray jets are not steady long-term structures; the structure varies, indicating that the reheating processes have no preference for a particular precession phase or distance from the binary core. Three observations made within about five days in 2001 May, and a 60-ks observation made in 2003 July, show that the variability of the jets can be very rapid, from time-scales of days to (possibly) hours. The three 2001 May images show two resolved knots in the east jet getting brighter one after the other, suggesting that a common phenomenon might be at the origin of the sequential reheatings of the knots. We discuss possible scenarios and propose a model to interpret these brightenings in terms of a propagating shock wave, revealing a second, faster outflow in the jet.

Key words: binaries: close – stars: individual: SS 433 – ISM: jets and outflows – radio continuum: stars.

1 INTRODUCTION

SS 433 is one of the most powerful and most studied jet sources in our Galaxy. It is a high-mass X-ray binary system located at a distance of about 5 kpc; e.g. 4.85 ± 0.2 in Vermeulen et al. (1993a); 4.61 ± 0.35 in Stirling et al. (2002); the most recent and likely estimate is 5.5 ± 0.2 in Blundell & Bowler (2004). The nature of the accreting compact object, either black hole (BH) or neutron star (NS), is still controversial. The most remarkable feature of the source is the presence of bipolar, precessing, mildly relativistic jets. These jets are observed at wavelengths from radio to X-rays and have been widely studied over about 30 years.

The geometry of the jets is well described to first order by the so-called 'kinematic model' (Abell & Margon 1979; Milgrom 1979; Hjellming & Johnston 1981; see Eikenberry et al. 2001; Stirling et al. 2002 for an update): the system is ejecting matter in the form of two antiparallel narrow jets, with an opening angle less than 5°. These jets precess in a 21° half-opening angle cone with a period of about 162.4 d (e.g. Eikenberry et al. 2001). The individual jet components move ballistically away from the system. The angle between the precession axis and the line of sight is about 78°, and the projection of the jets on to the plane of the sky results in a twisted trace. A velocity of $\sim 0.26c$ has been inferred from Doppler-shifted optical emission lines in the thermal component of the jets. The velocity of the jets seems to be stable, although a $\lesssim$15 per cent symmetrical scattering in the Doppler shifts of the optical lines (see Eikenberry et al. 2001) can be interpreted as an actual scatter of the velocity of the optical emitting jet component, i.e. at least up to distances of $\sim 10^{15}$ cm from the binary core, where the optical emission lines originate (e.g. Shaham 1981).

SS 433 is the only known galactic relativistic jet source to reveal the presence of baryonic matter in the jets, in the form of emission lines, both in optical and X-rays (e.g. Margon et al. 1979; Kotani et al. 1994), from thermal gas. The model developed and generally accepted to describe the emission of the thermal component of the jets is the 'adiabatic cooling model' (Brinkmann et al. 1991; Kotani et al. 1996; see also Marshall, Canizares & Norbert 2002). The temperature and the density of the jet gas decrease with increasing distance from the binary core. Close to the binary core, at distances less than 10^{11}–10^{12} cm, the jet gas is at a temperature of about 10^8 K (consistent with the temperatures of the inner regions of the accretion disc), and emits in the X-ray band. Subsequently the gas in the jets cools; at distances of about 10^{15} cm from the core the temperature is of the order of 10^4 K and the gas emits optical radiation. Based on the adiabatic cooling model, beyond this point the gas should be too cool to emit thermally optical or X-ray radiation. An alternative model has been proposed in which a high-temperature plasma emitting in X-rays coexists with clumps of cold matter emitting optical lines (Bodo et al. 1985; Brinkmann et al.

⋆E-mail: migliari@science.uva.nl

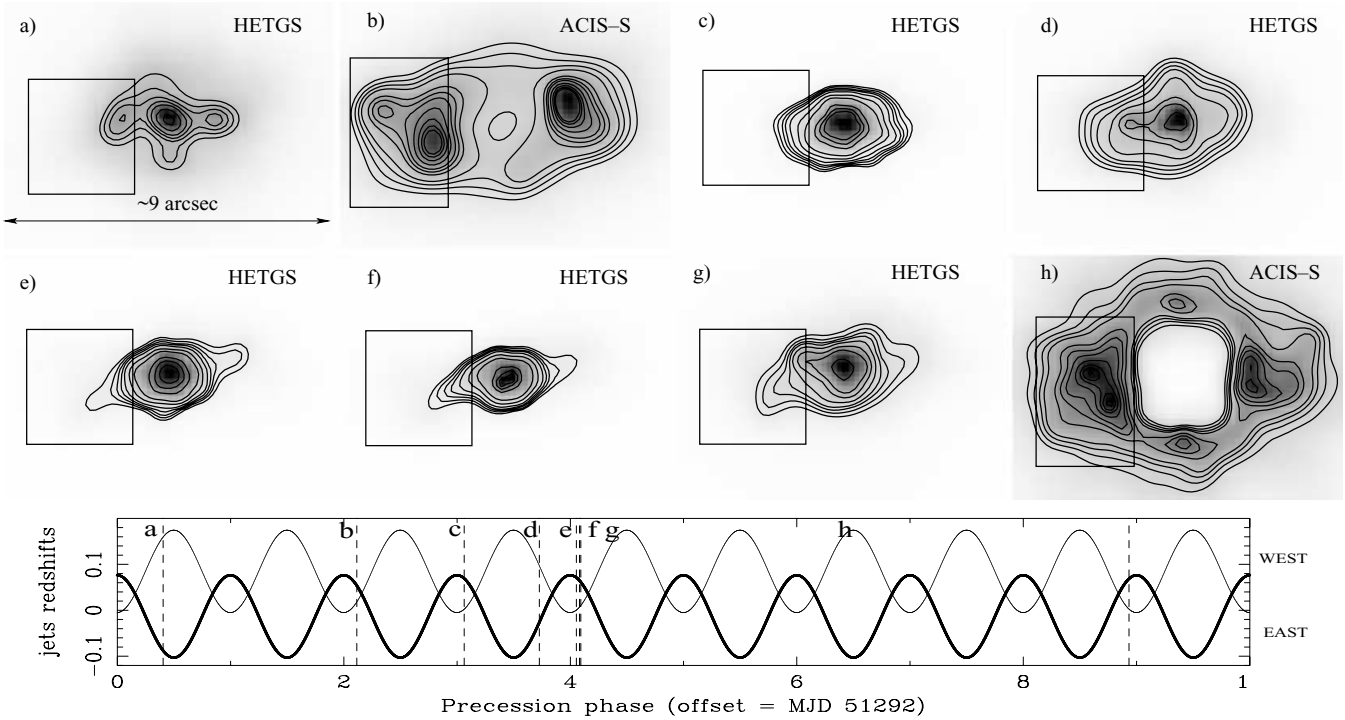

Figure 1. Upper panels: Smoothed zeroth-order HETGS and ACIS-S images of all the *Chandra* observations of SS 433: see Table 1 for details on each observation. The contour levels of HETGS images are normalized to the exposure time of (g) which has contours at 2.5, 3, 3.5, 4, 5, 7, 10, 20, 27, 34 counts per rebinned and smoothed pixel. The contour levels of ACIS-S observations are normalized to the exposure time of observation (h) which has contours at 4, 5, 6, 7, 10, 12, 14, 17, 20, 22, 24. The colour scales of the pixel images are normalized to the counts at the peak of each image. The regions superimposed to the images have been used to calculate the count rates in the east arcsec-scale jets. The regions have the same area and the same physical coordinates (RA and Dec.) for all the images taken with the same instrument, but different between HETGS and ACIS-S observations. Lower panel: Redshifts of the east (thick line) and west (thin line) jets at the base of the jet versus precession phase. Ticks in the abscissa mark a complete precessing cycle, i.e. every 162.4 d. The precession phase is calculated based on ephemeris in Stirling et al. (2002): $\phi = [(\mathrm{obs(JD)} - 2440\,000.5) - 8615.5]/162.4$. We show with vertical dotted lines the (core) precession phases at the time the *Chandra* observations have been taken.

1988). Non-thermal (synchrotron) radio emission from the jets is observed at distances of 10^{15}–10^{17} cm from the binary core (e.g. Hjellming & Johnston 1981).

Recent observations, however, appear to contradict, at least partially, the predictions of the adiabatic cooling model. In an observation taken with the *Chandra* high-energy transmission grating spectrometer (HETGS), Marshall et al. (2002) first discovered arcsec-scale X-ray jets in SS 433. Further spatially resolved X-ray spectral analysis of the arcsec jets, using a *Chandra* advanced charge-coupled device imaging spectrometer (ACIS)-S observation, revealed highly ionized Doppler-shifted iron emission lines at distances of about 10^{17} cm from the binary core (Migliari, Fender & Méndez 2002). This indicated that *in situ* reheating of atoms takes place in the jet flow, which is still moving with (mildly) relativistic velocity more than 100 d after launch from the binary core. Migliari et al. (2002) also attempted to explain this reheating by means of shocks formed due to collisions of different blobs launched with a slightly different velocity at the same precession phase, i.e. a faster blob which catches up a slower blob ejected later.

In this paper we present all the currently available *Chandra* observations of SS 433. We report on the morphology and evolution of the extended X-ray emission regions and present evidence for long-term and daily variability of the arcsec X-ray jets, discussing possible physical scenarios.

2 OBSERVATIONS AND DATA ANALYSIS

We have inspected the images of all the *Chandra* observations of SS 433 to date: six HETGS and two ACIS-S observations. We show all the images in Fig. 1. We have analysed the observations with the standard tools in CIAO v 3.1. The images shown in Fig. 1 have been rebinned to one-sixteenth of the original pixel size and smoothed with the tool CSMOOTH, using a minimal significance signal-to-noise ratio of 3 and a Gaussian convolution kernel. The observations span about four years, from 1999 September 23 (Fig. 1a) to 2003 July 10 (Fig. 1h), with exposure times from 9.7 ks to 58.1 ks (see Table 1). In the lower panel of Fig. 1 we show the redshifts due to the precession of the east and the west jets as a function of time. The dotted lines indicate the days the observations have been taken. Note that these redshifts refer to the matter launched at the base of the jets, close to the binary core. The outer parts of the arcsec-scale jet analysed in this work (see below) and indicated by the regions in the upper panels of Fig. 1 have a different precession phase (and thus redshift) than the one indicated by the dotted line in the lower panel. Matter in the jet at those distances from the core (about 10^{17} cm) has been launched 100–200 d before the observation was taken, and therefore with a precession phase corresponding to 1–1.5 precession cycles before (using the ephemeris in Stirling et al. 2002). For each observation we have estimated the count rate of the core (see Sections 2.1.1 and 2.2.2) and extracted the count rate in a region of the east jet (Fig. 1,

Table 1. Observation (referring to Fig. 1); *Chandra* instrument; date of observation; exposure time; orbital phase of the binary from Dolan et al. (1997): [obs(JD) − 2450 023.69]/13.08; precession phase of the jet based on Stirling et al. (2002; see Fig. 1); background subtracted count rates of the core as estimated from the fit of the energy spectra for the HETGS observations and from the readout streak for the ACIS observations (see Section 2.1.2 for details); background subtracted count rates of the east jets of all the *Chandra* observations of SS 433 estimated in the regions shown in the upper panel of Fig. 1; net count rates in the regions shown in the upper panel of Fig. 1, after the subtraction of the contribution of the core (see Section 2.2). Uncertainties are 1σ statistical errors.

Obs.	Instrument	Date	Exp. (ks)	Orbit. phase	Prec. phase	core (counts s^{-1})	east jet measured (counts s^{-1})	Δeast jet (counts s^{-1})
a[1]	HETGS	1999 Sept. 23 (MJD 51444)	28.6	0.664	0.420	1.442	0.0298 ± 0.0010	0.0036 ± 0.0014
c	HETGS	2000 Nov. 28 (MJD 51876)	22.7	0.618	0.080	0.557	0.0282 ± 0.0011	0.0183 ± 0.0013
d	HETGS	2001 March 16 (MJD 51984)	23.4	0.980	0.748	1.876	0.0598 ± 0.0016	0.0246 ± 0.0021
e	HETGS	2001 May 8 (MJD 52037)	19.6	0.005	0.072	0.363	0.0295 ± 0.0012	0.0234 ± 0.0013
f	HETGS	2001 May 10 (MJD 52039)	18.5	0.147	0.083	0.234	0.0293 ± 0.0013	0.0254 ± 0.0014
g[2]	HETGS	2001 May 12 (MJD 52041)	19.7	0.300	0.096	0.846	0.0391 ± 0.0014	0.0238 ± 0.0017
b[3]	ACIS-S	2000 June 27 (MJD 51722)	9.7	0.890	0.130	2.3	0.0803 ± 0.0028	0.0588 ± 0.0032
h	ACIS-S	2003 July 10 (MJD 52830)	58.1	0.641	0.956	8.8	0.0918 ± 0.0013	0.0132 ± 0.0018

For a more detailed analysis see [1]Marshall et al. (2002); [2]Namiki et al. (2003); [3]Migliari et al. (2002).

Table 2. Observation (referring to Fig. 1); equivalent neutral hydrogen column density $N_{\rm H}$; power-law photon index Γ; normalization of the power-law $N_{\rm PL}$; best-fitting χ^2/d.o.f.; unabsorbed flux F in the range 2–10 keV [except observation (g). The uncertainties are 1σ statistical errors.]

Obs.	$N_{\rm H}$ ($\times 10^{22}$) (cm^2)	Γ	$N_{\rm PL}$($\times 10^{-2}$) (ph cm^{-2} s^{-1})	χ^2/d.o.f.	F_{2-10}($\times 10^{-11}$) (erg cm^{-2} s^{-1})
a[1]	0.95	1.35	1.5	–	10.91
c	1 (fixed)	1.87 ± 0.05	1.03 ± 0.04	1486/1148	3.0 ± 0.2
d	1 (fixed)	1.47 ± 0.02	2.07 ± 0.04	978/988	13.36 ± 0.2
e	1 (fixed)	1.91 ± 0.08	0.68 ± 0.04	1068/938	1.9 ± 0.1
f	1 (fixed)	1.94 ± 0.11	0.46 ± 0.04	116/230	1.2 ± 0.1
g[2]	1.31 ± 0.06	1.40 ± 0.04	1.18 ± 0.07	2312/1964	8.7[3]

[1] ; [2]From Namiki et al. (2003); [3]The flux has been estimated in the range 1–10 keV.

upper panels). In the HETGS observations the regions have the same area and are at the same distance (centred at about 2 arcsec) as the four central brightest rebinned pixels in the smoothed image. In the two ACIS-S observations we fixed the coordinates (RA and Dec.) of the regions and chose a slightly bigger area in order to cover the knots observed in the jets. All the quantitative analysis in this work, such as the extractions of counts and count rates, has been done using the original images (i.e. not rebinned and not smoothed) in the 0.5–10 keV energy range. In Table 1 we report the background subtracted count rates in the core and in the east jet regions, with 1σ statistical errors, of all the observations. The count rates of the ACIS observations are much higher than the HETGS observations mostly because of the higher sensitivity of the instrument by about a factor of 4.

2.1 Estimate of the core count rates

2.1.1 HETGS observations

All the *Chandra* images shown in Fig. 1 are affected by pile-up. Therefore, in the case of the HETGS observations we have estimated the count rates from the unresolved core of SS 433 (which dominates the X-ray emission from the source) by analysing the dispersed energy spectra, which are not affected by pile-up. We have extracted the first-order (± 1) medium energy grating (MEG) and high energy grating (HEG) spectra following the standard procedures, using CIAO v. 3.1. We have analysed the combined MEG and HEG spectra in the range 0.8–8.0 keV. As in this work we are mainly interested in the estimate of the total flux in each spectrum, which is dominated by the broad continuum, we did not concentrate our attention on the weaker emission lines. We have rebinned the data in order to have a minimum of 20 counts per energy bin. The best-fitting model for the continuum in all the HETGS observations is a power law corrected for photoelectric absorption. We have added narrow Gaussian emission lines to this model for the spectrum of observation (d) to fit the strongest lines with residuals larger than 4σ, namely at about 1.85 keV, 1.98 keV, 6.30 keV and 6.59 keV. Since weaker emission lines below a few keV may still contribute to the actual value we measure of the absorption column density, we have fixed it to a reasonable value of $N_{\rm H} = 10^{22}$ cm^{-2}, which is consistent with that found by Marshall et al. (2002) and Namiki et al. (2003). In Table 2 we report the best-fitting parameters of the continuum of each spectrum and the unabsorbed flux in the 2–10 keV range. For observations (a) and (g) the values are those in Marshall et al. (2002) and Namiki et al. (2003), respectively. In Fig. 2 we show, as an example, the energy spectrum with the residuals with respect to the model of observations (c). Although the parameters of the power-law component shown in Table 2 may be considered as approximate estimates of the physical parameters of the source, comparing the fluxes we obtained with our fits and the fluxes derived from the more detailed analysis in Marshall et al. (2002) and Namiki et al. (2003), we find that they are consistent within less than 10 per cent (8 and 5 per cent, respectively, for the two observations). We have used the 2–10 keV unabsorbed fluxes of the spectra to estimate with PIMMS the 0.5–10 keV count rates we expect from the unresolved core of the source in the *Chandra*

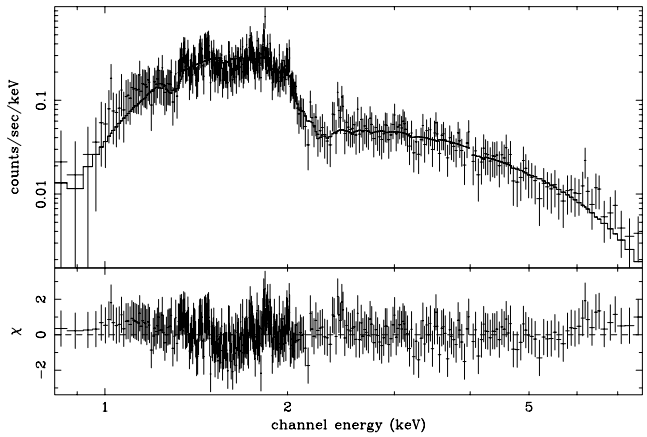

Figure 2. Energy spectrum of observation (c) with the residuals with respect to the fit with an absorbed power-law model. See Section 2.1.1 for details.

HETGS images, dividing by a factor of 4 the expected count rates in the ACIS-S. The core count rates are reported in Table 1.

2.1.2 ACIS observations

The ACIS observations are also affected by pile-up, but there is no dispersed spectrum. Therefore, we have estimated the 0.5–10 keV count rate of the core by analysing the photons in the readout streak, which should be unaffected by pile-up. We have extracted the background subtracted counts in a rectangular region with $n \times m$ pixels covering the readout streak (where we chose $m = 20$ in a direction perpendicular to the streak and $n = 280$ as the number of row-pixels in the direction of the streak) and divided these counts by the effective exposure time for the readout streak data, calculated as follows. The time to read out one row of pixels in a direction perpendicular to the readout streak is 40 μs. The effective exposure time per frame for the streak region is then $n \times 4 \times 10^{-5}$ s. The number of frames of an observation is the ratio between the actual exposure time and the frame time (which is 3.2 s for all the SS 433 observations). The core count rates of the ACIS observations are shown in Table 1.

2.2 Estimate of the contribution of the core to the measured count rates in the east jet

Using the actual count rate we expect from the core of SS433 in each observation, we have calculated the contribution of the core in the regions where we have estimated the count rates of the east jet. For each observation we have created the 3-keV point spread function (PSF) in the core position and normalized it to the total counts in the core. We have estimated the count rate of the normalized PSF in the regions shown in Fig. 1. The contribution of the core to the count rates in these regions (which is ∼2 per cent of the total core count rate), together with the total count rates we measured from the image, and the residuals, are shown as a function of the total count rates of the core, for the HETGS observations, in Fig. 3 (see also Table 1). It can be seen that the wings of the core PSF may contribute up to 50 per cent of the flux measured in the eastern jet. However, a constant model fit to the residuals, corresponding to a steady eastern jet, can be rejected at the >99.9 per cent level (χ^2/d.o.f. = 169/5). The rejection level remains at >99.9 per cent (χ^2/d.o.f. = 16.7/4) even if the most strongly deviating point, that of observation (a) (1.44 core count s^{-1}), is removed. This establishes

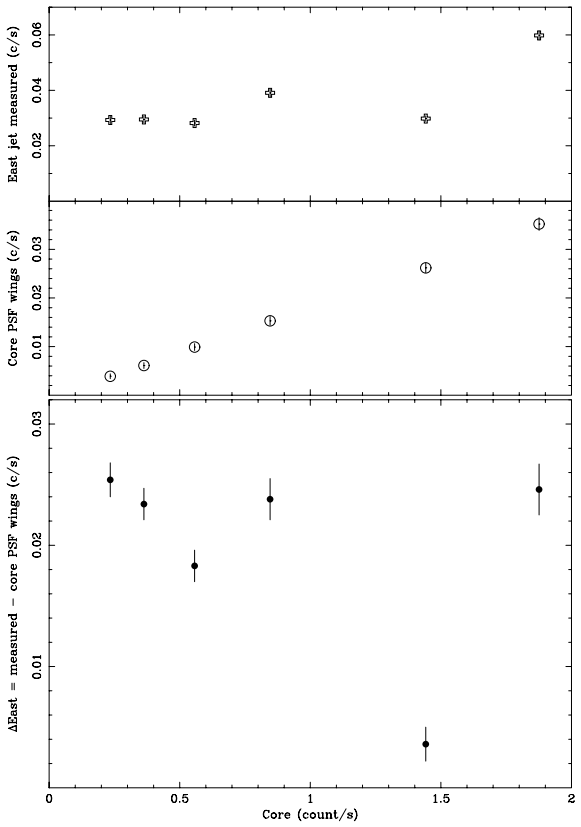

Figure 3. Count rates in the east jet regions (see Fig. 1) of the HETGS observations as measured in the image (upper panel), due to the contribution of the bright core (middle panel) and the residuals (lower panel), as a function of the total count rates of the core. The error bars are 1σ statistical errors.

that the eastern jet is significantly variable in a way which cannot be explained simply by the PSF of the variable core.

3 RESULTS

A simple model was presented in Migliari et al. (2002) to explain the reheated arcsec X-ray jets of SS 433 as 'average' long-term structures, with line energies representing the mean Doppler shifts on each side of the jet. Imaging as presented here with a larger sample of observations suggests a considerably more complex picture.

3.1 Morphology

In order to study the asymmetries of the extended emissions in the X-ray images shown in Fig. 1, we have analysed the projections of the 0.5–10 keV images in three directions: north–south (N–S), east–west (E–W) and north-west–south-east (NW–SE). The angular width of the projections is <0.1 arcsec, i.e. much less than the pixel size of the images. Dividing the counts in the N–S and E–W projections by the counts in the NW–SE projection, and comparing these ratios to what was expected from the PSFs of the images, we are able to investigate not only the E–W jet structure, but also the possible presence of an extended X-ray emission in the equatorial direction (extended radio emission in a direction approximately perpendicular to the jets has been observed on milliarcsec scales; Paragi et al. 1999; Blundell et al. 2001). In Fig. 4 (central image of the upper panels) we show a typical PSF image and the ratios of the

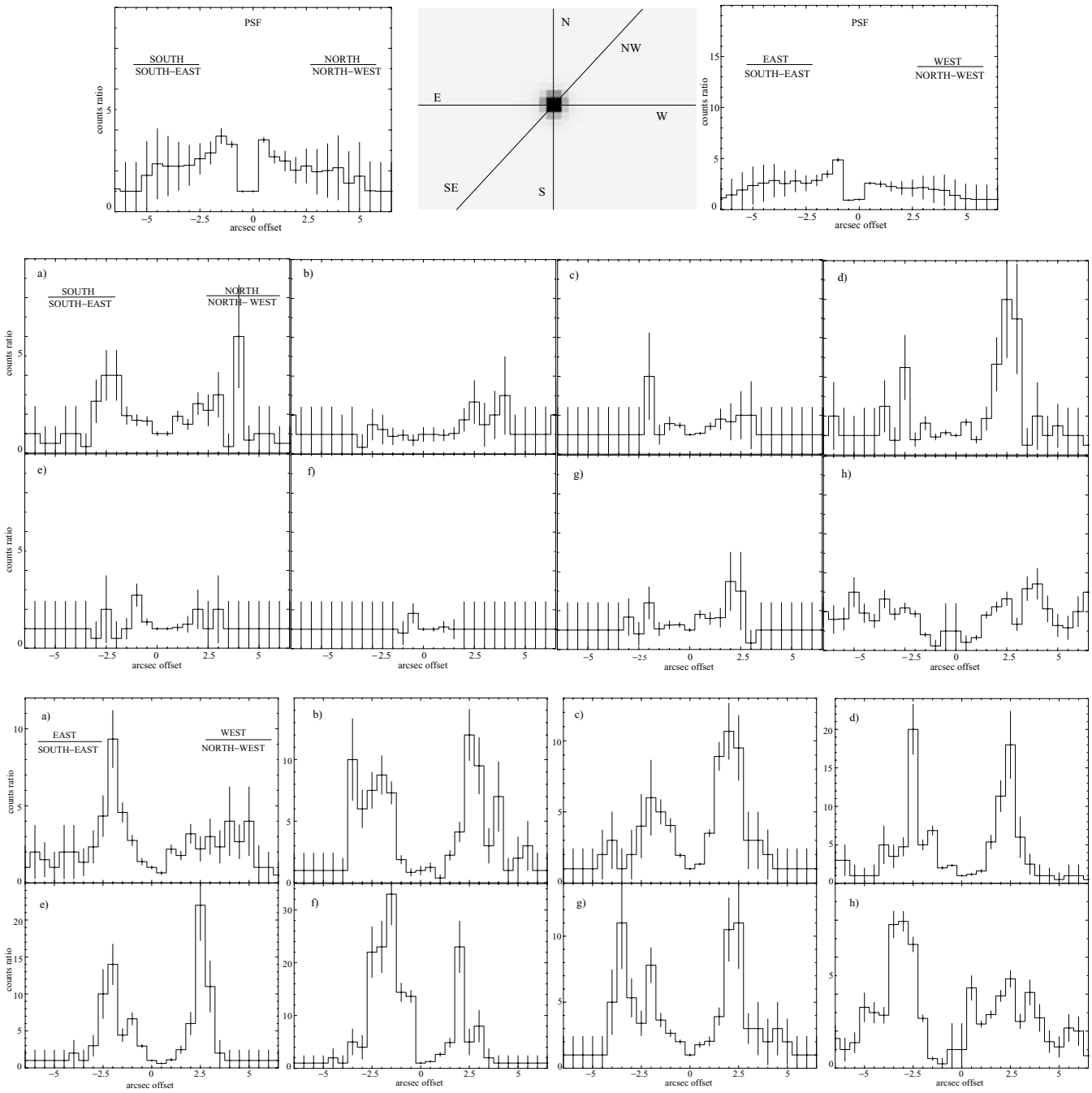

Figure 4. Upper panels: Image of the PSF with the three projections we have used to analyse the asymmetries in the *Chandra* images (centre) and counts ratios of the N–S (left) and E–W (right) by the NW–SE projection as a function of the distance from the centre of the PSF image. Middle panels: Counts ratios of the N–S by the NW–SE projection versus offset from the centre of the images (see Section 3.1) of all the *Chandra* images shown in Fig. 1. All the plots are on the same scale. Lower panels: Counts ratios between the E–W and the NW–SE projection versus the offset from the centre of the images of all the *Chandra* images shown in Fig. 1. Note the different scales in the ordinate of the plots.

projections. The PSFs at 3 keV have been extracted with the tool MKPSF and normalized to the total counts of the image (Table 1; see Sections 2.1.1 and 2.1.2). On either side of the PSF image of Fig. 4 we show the counts ratios of the N–S/NW–SE and E–W/NW–SE projections versus the offset from the brightest pixel in the image. In the middle and lower panels of Fig. 4 we plot, for each observation, the counts ratios (not background subtracted) as a function of the offset from the core of the source, showing the extended asymmetries in the N–S and E–W direction, respectively. The core position in each image has been chosen as the brightest pixel in the case of HETGS images, and the pixel in the centre of the pile-up distortion in the case of ACIS-S images. In order to avoid divisions by zero when no counts are present in the projected pixel, we assign arbitrarily to the pixel a value of 1 ± 1 count. Note that, due to precession, the jets are not always perfectly in the E–W direction and the histograms in Fig. 4 reflect only the component in this direction. If we compare the plots in the middle panels to the plot of the PSF in the upper left panel, although there seem to be indications

for an extended emission in a direction perpendicular to the jets in observations (a), (d) and (h), the asymmetries are consistent within errors with asymmetries of their PSFs. All the observations show actual extended X-ray emissions in the E–W direction, not related to asymmetries of the PSF image. These extended jet emissions have been already shown – and quantified – for the east jets in Fig. 3 and Table 1.

3.2 Variability of the X-ray jets

3.2.1 Long-term

Comparison of our two ACIS images (Fig. 1b and h), obtained three years apart, indicates X-ray structural changes. Including archival *Chandra* observations we now have a sample of eight images of the arcsec X-ray jet structure (Fig. 1). These images (see also Fig. 3) indicate that the arcsec-scale X-ray jets do not have a static and long-term structure. The jet structure appears, instead, to be continuously evolving. In Table 1 we report the count rates estimated in the core and in the regions of the east jet indicated in the upper panel of Fig. 1, for all the *Chandra* observations. In the lower panel of Fig. 3, we plot the count rates from the extended emission in the east regions after the subtraction of the core contribution (see Section 2.2). The plot shows significant variations in the X-ray emission from the east jet. The east jet count rates change significantly between different observations and even between observations with approximately the same precession phase [e.g. observations (c) and (f)], implying no correlation between the reheating process and the precession phase of the jets. In particular in observations (e), (f) and (g), taken within approximately 5 d, basically with the same precession phase, we see very fast variations of the arcsec structure (see Section 3.2.2) with bright regions located at different distances from the binary core. This indicates that reheating at arcsec scales does not happen at a particular distance from the binary. Similar results, albeit on smaller physical scales, have recently been reported by Mioduszewski et al. (2004) based on Very Long Baseline Array (VLBA) radio observations of the milliarcsec-scale jets of SS 433, in which they show radio knots getting brighter at different distances from the core. This is contrary to the previous idea of a fixed (radio) 'brightening zone' around 50 milliarcsec (Vermeulen et al. 1993a).

3.2.2 Daily

Inspecting three ∼20-ks zeroth-order HETGS images taken over a period of ∼5 d (see Fig. 1e, f and g), we observe rapid and significant changes in the arcsec-scale X-ray jets on time-scales of $\leqslant$2 d. The structural variations of the jets of these three observations can also be observed in the lower panels of Fig. 4 (e, f and g) where the east jet counts at ∼−2 arcsec increase from observation (e) to observation (f) and then decrease again in (g). Note that since we are observing the counts projected in the E–W direction, which is not the direction of blob B, we are following mostly the evolution of blob A. In Fig. 5 we show the contour plots of the observations (e), (f) and (g) superimposed to the precession trace of the jets, shifted in phase by $\Delta\phi \sim -0.1$ (more details are presented in Blundell & Bowler 2004; see also Stirling et al. 2004) with respect to the model in Stirling et al. (2002). (Nevertheless, with or without this small shift the results of this work are not significantly affected, either qualitatively nor quantitatively.) The contour levels correspond to the smoothed image. The minimum-significance signal-to-noise ratio in the smoothing procedure has been decreased from 3 (as in Fig. 1) to 2.5 in order to emphasize the knot structures in the jets. The knot structure is observable when the counts of the source and the resolution and the sensitivity of the instrument are high enough (e.g. ACIS-S observations in Fig. 1b and h and the nearly 30-ks HETGS observation in Fig. 1a). We have chosen the size of the circular regions in which we estimate the counts, as large as the original-size pixel of the image, and such that outside the circle regions the counts per rebinned-pixel of a point source distributed on the image by the

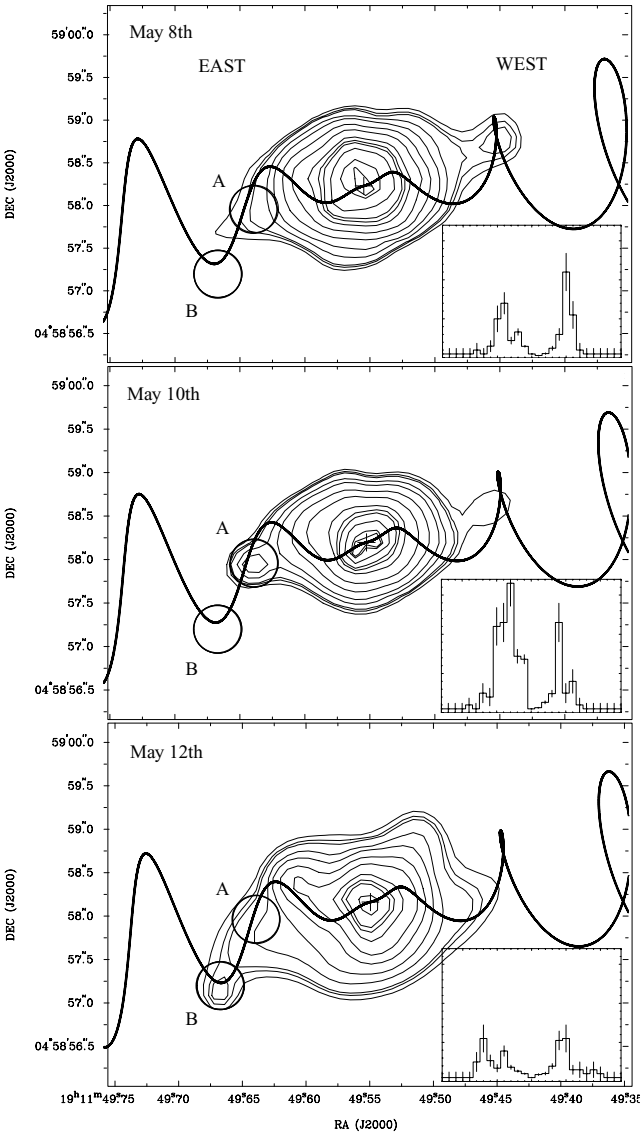

Figure 5. Three ∼20-ks zeroth-order HETGS images of SS 433, taken every 2 d on 2001 May 8 (top), May 10 (middle) and May 12 (bottom). Images are rebinned to one-sixteenth of the original pixel size and smoothed. Contour levels are 2.7, 3, 3.2, 4, 5, 7, 10, 15, 18, 20, 25, 34, 37 counts per rebinned-pixel for the May 12 observation and normalized to this for small changes in exposure times (less than 6 per cent) in the other two observations. The twisted precession trace as predicted from Stirling et al. (2002), with the small phase correction (see Section 3.2.2), is superimposed on the images. The lower-right panels show the histograms of the three observations as in Fig. 4 (but here on the same scale) the variations of the source in the E–W direction (see Section 3.1). These contour images indicate a brightening of the east jet and a rapid fading in the west jet. We associate the X-ray variability with the brightening and fading of unresolved discrete components (knots) projected along the precession trace. The geometry at this epoch is sketched in Fig. 6.

Table 3. Background subtracted counts, with 1σ statistical errors, in region A and region B (see Fig. 4) for the three 2001 May observations. The counts are calculated in the 0.5–10 keV energy range and normalized to the exposure time of the 2001 May 12 observation.

Obs.	A (counts)	B (counts)
2001 May 8	46.1 ± 6.8	29.0 ± 5.4
2001 May 10	75.2 ± 8.9	38.1 ± 6.4
2001 May 12	62.8 ± 7.9	57.8 ± 7.6

PSF are less than the 25 per cent of the counts per rebinned-pixel at the peak. We observe a knot getting brighter from May 8 to May 10 (knot A) and subsequently on May 12 we see it apparently moving, following the precession trace (knot B). This indicates that we are observing two knots lying on the precession trace, at different precession phases, which brighten up sequentially. To quantify these brightenings we have estimated the background subtracted counts in the circular regions A and B for these three observations (see Table 3). The counts have been normalized to the exposure time of the May 12 observation. Taking the counts in the regions on May 8 as a reference, we observe region A brightening about two days later and subsequently region B getting brighter, about four days later. Considering statistical errors, both brightenings are significant at the >99 per cent confidence level if we consider May 8 knots as a reference: knot A: May 10−May 8 = 29.1 ± 11.2, i.e. 99.1 per cent significance; knot B: May 12−May 8 = 28.8 ± 9.3, i.e. 99.7 per cent significance. (When testing against the null hypothesis of a constant model, the probability of obtaining a larger value of χ^2 is 3 per cent for knot A and 1 per cent for knot B.) Since (i) the core count rate decreases from May 8 to May 10 while the count rate of knot A increases and (ii) we observe a (albeit small) decrease in the count rate of knot A (which is closer to the core than knot B) from May 10 to May 12, while the count rate of knot B increases, and since the PSF of the core is about symmetric at those distances from the core, we are confident that we are observing actual variations in the jets, not directly related to contaminations of the PSF of the core.

3.2.3 Hour time-scale

Analysing the 60-ks ACIS-S observation of SS 433 (Fig. 1h) we have selected two regions of the image corresponding to the east (the region is smaller than the one shown in Fig. 1(h) and zoomed on the two knots clearly visible in the image) and the west jets. We have applied baricentre corrections and extracted the background subtracted light curves in these regions with a time bin of ∼6000 s, in the range 0.5–10 keV. We have fitted the two light curves with a constant and did a χ^2 test to check if they are consistent with a steady jet emission on time-scales of hours. The west jet is consistent with being steady. However, in the light curve of the east jet, although it does not show any systematic trend, we can reject a steady distribution at the 3.5 per cent level (the fit with a constant gives a reduced-$\chi^2 = 2.0$ with 9 d.o.f.). Assuming a variation in the east jet – the variation is marginally significant and needs to be confirmed – because of the signal propagation speed, the linear size of the emitting region should be smaller than $c \times \Delta t \sim 10$ s au, where $\Delta t \sim 60$ ks. We have also extracted the light curve, with the same time bin, of the readout streak of the image, to check the variability of the core. The core is consistent with being steady over the whole observation.

4 JET REHEATING: POSSIBLE SCENARIOS

Whatever the underlying explanation, the rapid variability indicates that the observed extended X-ray emission originates in physically small components which may be suffering shock acceleration, as we now consider. The lack of correlation with precession phase indicates an origin of this phenomenon in a more random process, e.g. the variability of the underlying accretion flow.

4.1 Internal shocks

The possibility of internal shocks (originally proposed by Rees 1978 for the radio galaxy M87) between 'blobs' ejected at almost the same precession phase with slightly different velocities (the mean speed of the thermal matter in the jet is ∼0.26c and might be scattered by ±15 per cent: Eikenberry et al. 2001; see also Blundell & Bowler 2004) can explain the arcsec-scale jet X-ray brightenings (Migliari et al. 2002). Knot brightenings similar to those described above in X-ray are also observed in the radio band on much smaller physical scales (e.g. Vermeulen et al. 1993a). Mioduszewski et al. (2004) have recently monitored with the VLBA the milliarcsec-scale variability of SS 433 for one-fourth of the jet precession cycle. In the 42 d of their radio monitoring we observe an average of a blob ejection every ∼6 d, with a peak of one every 2–3 d in the most active period. In 6 d the jet axis has moved, due to precession, by about 1.5°. With such a small angle, two ∼5°-size blobs (e.g. Begelman et al. 1980) can still interact with each other if the second blob has been launched faster than the first, although they move in slightly different directions. In the case of a blob with a velocity of 0.3c launched 6 d after a blob with a velocity of 0.2c, the second blob should reach the first at a distance of $\sim 10^{16}$ cm from the core. To explain knots getting brighter at distances of $\sim 10^{17}$ cm from the core, where we observe the arcsec-scale X-ray jets, the difference in the velocities of the blobs can be smaller and an 'internal shock' mechanism may explain what we observe in X-rays.

If this is the correct scenario and since we observe in both X-ray (Fig. 1) and radio images (Mioduszewski et al. 2004) knots getting brighter with no dependence on distance or precession phase, the velocity scattering of the ejections should be more or less random with respect to periodicities of the system. Therefore, we must note that the fact that the first time the arcsec X-ray jets of SS 433 have been 'monitored' with three observations within about five days [observations (e), (f), (g)] shows what seems to be a 'sequence' of events where two knots get brighter one after the other (knot A, and then knot B in Fig. 5), is at least curious and worth investigating. Moreover, Mioduszewski et al. (2004) show that radio knots can get brighter at distances of $\sim 10^{15}$ cm from the core. This distance seems too short for an internal shock scenario which considers two blobs launched 6 d (but even 2–3 d) apart with a velocity difference of only ∼15 per cent (i.e. a factor of more than 2 in the speed of one of the blobs is still needed). Based on this, we suggest that something else might be at the origin of the knot brightening in the jets, which can account for both large and small-scale observations and for the sequence of brightenings observed in X-rays. We suggest a new scenario in which the slower-moving clouds are energized erratically by a more powerful, faster, unseen flow.

4.2 Proposed scenario: an underlying faster outflow

In Fig. 5 we observe two knots, corresponding to regions A and B. The kinematic model tells us the projection on to the plane of the sky of the knots ejected. By identifying these knots on the precession

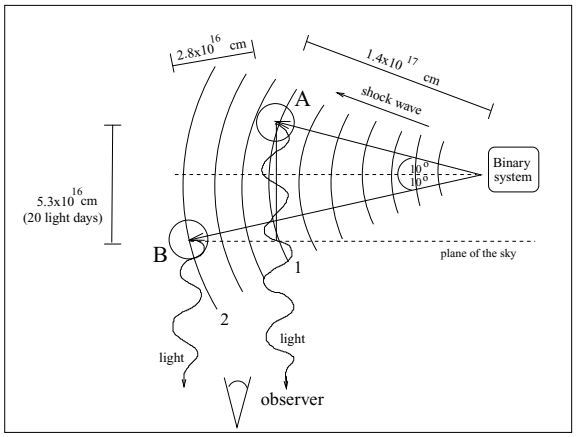

Figure 6. Sketch of the orientation of the east jet of SS 433 at the time of the observations in Fig. 5 (assuming a distance of 5 kpc). Knot B was observed to brighten <2 d after knot A. We propose that a shock wave propagates from the binary core (on the right) through the jet and hits first the knot A (1) and then the knot B (2). Knot A is about 20 light days farther from us than knot B. We see knot B getting bright at least 2 d later than knot A. This means that the shock wave has to travel from knot A to knot B within about 22 d, with a velocity of $\gtrsim 0.5c$.

trace we can de-project the image and give a three-dimensional position of the knots. A sketched view from 'above' of the east jet as observed in Fig. 5, is shown in Fig. 6. As described in Section 4.1, we assume that a shock wave forms and travels at relativistic velocities (faster than the velocity of the knots which is about $0.26c$) through the jet. Assuming a distance to the source of 5 kpc, we can now estimate the time-scales and spatial scales involved in such shock events. In the May 10 image of Fig. 5 we see that knot A is about in the middle of the 'descending' trace at a distance of about 1.4×10^{17} cm from the binary core. Following the kinematic model, we infer that knot A was ejected about 200 d before the observation, and is moving away from us at an angle to the line of sight of $\sim 100^\circ$ (see Fig. 6). The May 12 image in Fig. 5 shows knot B at the bottom of the precession trace at a distance of about 1.7×10^{17} cm from the core. Knot B was ejected from the binary system about 40 d earlier than knot A, and is moving towards us with an angle to the line of sight of $\sim 80^\circ$ (see Fig. 6). The shock wave interacts first with knot A and then with knot B. At the time at which the shock interacts with knot A, this was about 20 light days farther from us than knot B. Therefore, the shock wave has to travel the projected distance between the two knots in about 22 d (we observe knot B brightening no more than two days after knot A). In order to observe the brightenings of the two components within two days, the shock has to travel with a velocity of $v \sim 0.5c$ [the velocity is $\sim 0.6c$ if we use the most recent estimate for the distance of 5.5 kpc (Blundell & Bowler 2004)]. Note that the value we have inferred of $0.5c$ might be considered as a lower limit because (i) the positions of the knots on the precession trace were chosen by eye from Fig. 5; any other position on the 'descending' trace of any of the two knots would decrease the light days difference to us between the knots and thus increase the velocity of the shock; (ii) the brightening of knot B after knot A might have happened any time within the 2 d between the May 10 and May 12 observations, thus, since usually the radiative lifetime of the thermal knots is of the order of two days or more (Vermeulen et al. 1993b), we may consider 2 d as an upper limit in time. What we observe is therefore consistent with being due to a shock wave which travels from the binary core downstream in the jet with an inferred velocity of $\gtrsim 0.5c$. This shock should be broader than the thermal jet collimation angle of $\sim 5^\circ$ as inferred by optical spectral analysis at distances of 10^{15} cm from the core, because it has to brighten up two knots with different precession phase (i.e. angle to the line of sight). Since the velocity of this shock wave is greater than that observed for the moving components (including the possible scatter of 15 per cent; Eikenberry et al. 2001), it seems to correspond to an unseen second component to the outflow.

5 DISCUSSION

Eight X-ray *Chandra* images of SS 433 revealed that its arcsec X-ray jet structure varies very rapidly, possibly as short as hour time-scales. The observations show that the reheating processes, which are at the origin of the X-ray jets, have no preference for a particular precession phase of the jet or distance from the binary core. In particular, a sequence of three images made within about five days show two knots in the east jet getting brighter sequentially, suggesting that both knots are responding to the same phenomenon.

Radio changes, like those described above in X-rays, have been observed also on smaller scales (of the order of 10^{16} cm from the binary core; Vermeulen et al. 1993a; see also Mioduszewski et al. 2004). X-ray images indicate that the shocks which may cause those changes in radio continue also on larger scales. Moreover, since the knots fade significantly on time-scales of days (knots that emit optical lines have a typical lifetime of ~ 2 d: Vermeulen et al. 1993b; Fig. 5 also shows a knot in the west jet fading in a few days), and assuming that the brightening of the two knots A and B is responding to the same underlying phenomenon, a frequent 'pumping' of such shocks is required. Put another way, if the core energy source switches off, we would expect the arcsec-scale X-ray jets to fade away very rapidly.

Another possibility, other than a single shock wave, is a sequence of shocks, like a wave train. In this case there is the possibility that knot A and knot B have been brightened by two different crests of the same wave train. If on May 8 the first crest has already passed knot A, it has to be since about 2–6 d, which is the range in which we expect the knot to fade away almost completely. Therefore, if this first crest brightens knot B on May 12, it takes ~ 8 d to travel 2.8×10^{16} cm (see Fig. 6), implying a slightly slower shock wave with a velocity of $\sim 0.4c$. If a second crest of the wave train brightens knot A on May 10, the spacing between the crests is a few days.

The possible existence of an underlying, energizing flow which is not directly observed and has a velocity greater than the observed components might have seemed speculative only a few years ago. However, recent detailed studies of the jets from two neutron star X-ray binaries, Sco X-1 (Fomalont et al. 2001) and Cir X-1 (Fender et al. 2004), have revealed precisely this phenomenon. In Sco X-1, Fomalont et al. (2001) observed compact radio jet lobes moving outward with a velocity of at most $0.57c$. They observed that flares in the core and in the lobes are correlated and indicate an energy flow moving from the core within the jet beams with a speed of $>0.95c$. A similar behaviour has been observed in Cir X-1. Fender et al. (2004) observed an ultrarelativistic energy flux moving from the core with a velocity of $>0.99c$ and consequently brightening two radio jet lobes of the approaching jet which are observed to move much slower. The two lobes which get brighter in Cir X-1 are not precisely aligned with the core (although a very small angle of the jet to the line of sight, as Cir X-1 seems to have, would amplify the apparent misalignment), further supporting the idea that the second component relativistic jet flow might be less collimated than the slower discrete knot ejections observed to be getting brighter. The

observations presented here challenge our current understanding of SS 433, which has been considered one of the best-known galactic sources to date.

ACKNOWLEDGMENTS

We thank the referee, Herman Marshall, for insightful comments which helped to improve the paper. SM wishes to thank Gabriele Ghisellini for stimulating discussions.

REFERENCES

Abell G. O., Margon B., 1979, Nat, 279, 701
Begelman M. C., Sarazin C. L., Hatchett S. P., McKee C. F., Arons J., 1980, ApJ, 238, 722
Blundell K. M., Bowler M. G., 2004, ApJ, 616, L159
Blundell K. M., Mioduszewski A. J., Muxlow T. W. B., Podsiadlowski P., Rupen M. P., 2001, ApJ, 562, L79
Bodo G., Ferrari A., Massaglia S., Tsinganos K., 1985, A&A, 149, 246
Brinkmann W., Fink H. H., Massaglia S., Bodo G., Ferrari A., 1988, A&A, 196, 313
Brinkmann W., Kawai N., Matsuoka M., Fink H. H., 1991, A&A, 241, 112
Dolan J. F. et al., 1997, A&A, 327, 648
Eikenberry S. S., Cameron P. B., Fierce D. M., Kull D. M., Dror D. H., Houck J. R., 2001, ApJ, 561, 1027
Fender R., Wu K., Johnston H., Tzioumis T., Jonker P., Spencer R., van der Klis M., 2004, Nat, 427, 222
Fomalont E. B., Geldzahler B. J., Bradshaw C. F., 2001, ApJ, 553, L27
Hjellming R. M., Johnston K. J., 1981, Nat, 290, 100
Kotani T. et al., 1994, PASJ, 46, L147
Kotani T., Kaway N., Matsuoka M., Brinkmann W., 1996, PASJ, 48, 619
Margon B., Stone R. P. S., Klemola A., Ford H. C., Katz J. I., Kwitter K. B., Ulrich R. K., 1979, ApJ, 230, L41
Marshall H. L., Canizares C. R., Norbert S. S., 2002, ApJ, 564, 941
Migliari S., Fender R., Méndez M., 2002, Sci, 297, 1673
Milgrom M., 1979, A&A, 76, L3
Mioduszewski A., Rupen M., Taylor G., Walker C., 2004, http://www. nrao. edu/pr/2004/ss433/
Namiki M., Kaway N., Kotani T., Makishima K., 2003, PASJ, 55, 281
Paragi Z., Vermeulen R. C., Fejes I., Spencer R. E., Stirling A. M., 1999, A&A, 348, 910
Rees M. J., 1978, MNRAS, 184, 61P
Shaham J., 1981, Vistas Astron., 25, 217
Stirling A. M., Jowett F. H., Spencer R. E., Paragi Z., Ogley R. N., Cawthorne T. V., 2002, MNRAS, 337, 657
Stirling A. M., Spencer R. E., Cawthorne T. V., Paragi Z., 2004, MNRAS, 354, 1239
Vermeulen R. C., Schilizzi R. T., Spencer R. E., Romney J. D., Fejes I., 1993a, ApJ, 270, 177
Vermeulen R. C. et al. 1993b, ApJ, 270, 204

This paper has been typeset from a TEX/LATEX file prepared by the author.